

# Total Internal Reflection Fluorescence Microscopy To Investigate the Distribution of Residual Bitumen in Oil Sands Tailings

Swapnali S. Shende,<sup>†</sup> Sarang Pendharker,<sup>‡</sup> Zubin Jacob,<sup>‡,§</sup> and Neda Nazemifard<sup>\*,†</sup>

<sup>†</sup>Department of Chemical and Materials Engineering, and <sup>‡</sup>Department of Electrical and Computer Engineering, University of Alberta, Edmonton, Alberta T6G 2V4, Canada

<sup>§</sup>Department of Electrical Engineering, Purdue University, West Lafayette, Indiana 47907, United States

**ABSTRACT:** A major waste byproduct of oil sands *in situ* extraction is oil sands tailings, which are a mixture of water, clay, and residual bitumen. These tailings represent a huge ecological footprint in the form of tailings ponds, which not only render large land areas unusable but also prevent reuse of water. The slow dewatering of the tailings ponds poses a major challenge to the industry. The presence of complex inorganic–organic bitumen–clay mixtures in these tailings contributes to this problem. Hence, understanding the nature of the bitumen–clay association and the effect of bitumen on clay particle–particle interactions is important for the development of more effective chemicals or processes to accelerate particle aggregation and sedimentation during dewatering. Previous studies that investigate these interactions used techniques that are sensitive only toward inorganic clay but not sensitive towards organic bitumen. Here, we use a high-resolution total internal reflection fluorescence (TIRF) microscopy to help identify the accurate location and distribution of bitumen in mature fine tailings (MFT) samples. We report the first adaptation of TIRF beyond cell biology for visualization of bitumen and its interaction with clay. The high signal-to-noise ratio of TIRF microscopy and a high contrast between the clay and residual bitumen provide images that reveal a wealth of information about the bitumen coverage on clay as well as clay–clay aggregates and how the bitumen positions itself within these aggregates. These images confirm the presence of hydrophobic fine clay agglomerates along with the hydrophilic clay particles in MFT. It is also observed that bitumen coats clay particles, bridges clay agglomerates, and is mostly absent as free bitumen in the bulk of the MFT sample. Our work paves the way for the use of nanophotonic tools in oil sands imaging and provides strategic suggestions for the development of better methods for clay sedimentation and bitumen recovery.

## 1. INTRODUCTION

Oil sands consist of mostly water, minerals, and bitumen.<sup>1</sup> The amount of oil sands deposits in Canada make it a country with

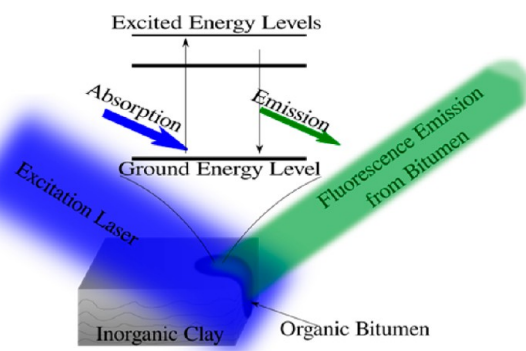


**Figure 1.** Fluorescence emitted by bitumen on illumination with an excitation laser. Clay does not show fluorescence, and hence, clay and bitumen show a high contrast in fluorescent images.

the third largest oil reserves in the world are mainly found in the Athabasca, Cold Lake and Peace River region of Alberta. Bitumen from oil sands has a higher viscosity, higher density, higher quantity of heavy metals, and lower hydrogen/carbon ratio in comparison to conventional crude oil.<sup>1</sup>

Oil sands are recovered from the ground by either surface mining or *in situ* technology. About 10% of the oil sands

reserves can be recovered using surface mining technique, which is much cheaper than the *in situ* technique.<sup>2</sup> Surface mining involves removing the overburden, digging the exposed oil sands, transporting the oil sands to the crushers, and then sending the crushed oil sands to the extraction plants. The hot-water extraction process is one of the techniques used for extracting oil from the oil sands. In this technique, oil sands are mixed with hot water to form a slurry, which is then sent to a separation vessel. Here, the slurry separates into 3 layers: a bottom layer consisting of sand, a middle layer consisting of clay, water and some sand and a top layer called a bitumen froth. The waste byproduct from the extraction process consisting of sand, clay, fine silt, and water are called tailings. It is sent to tailing ponds to allow sedimentation. Tailings are known to contain contaminants, such as naphthenic acids,<sup>3</sup> polycyclic aromatic hydrocarbons,<sup>4</sup> mercury, and trace metals,<sup>5</sup> which are harmful to the environment and therefore need to be mitigated. Over time, a top water layer is formed in the tailing ponds, which is recycled back to the extraction plant. The bottom layer eventually forms mature fine tailings (MFT), which has a solid content up to 30% (w/w) with the remainder being water. Further dewatering of MFT can take as long as 100 years.<sup>1</sup> Strict government regulations, economic constraints, and negative environmental impacts have urged

Received: March 30, 2016

Revised: June 1, 2016

Published: June 6, 2016

industries to increase the speed of tailings dewatering, water recycle, and tailings land reclamation. Various methods, such as adding gypsum to increase clay consolidation,<sup>6</sup> adding flocculants,<sup>7–9</sup> filtration, and drying, have been explored to increase the separation rate of water from solids to no avail. To increase the MFT settling rate, it is important to understand its components, their surface chemistry, and their surface interactions. Substantial research is being conducted in this area.

The slow settling of MFT and lowered bitumen recovery are mainly attributed to factors such as pH,<sup>10</sup> small clay particle size,<sup>11</sup> negative surface charge of clay,<sup>12</sup> gelation of clay,<sup>13</sup> types of clays,<sup>11,14–16</sup> and presence of the residual bitumen in tailings.<sup>2,1,17</sup> Residual bitumen ends up in tailings as a result of the bitumen–clay attachment in oil sands, which impairs the bitumen–air attachment during froth flotation.<sup>18–20</sup> A significant percentage of oil sands clays has organic material physically or chemically adsorbed onto its surface.<sup>2,15,16,21</sup> These clay–organic interactions take place at a 1–10 nm scale, but they impact the recovery and upgrading of bitumen on a much larger scale.<sup>22</sup> As a result of the nanoscale of these interactions and a lack of contrast, a bright-field optical microscope cannot be used to study these interactions. Various other techniques, such as X-ray photoelectron spectroscopy (XPS),<sup>23</sup> X-ray fluorescence (XRF) microscopy,<sup>24</sup> atomic force microscopy (AFM),<sup>16</sup> transmission electron microscopy (TEM),<sup>25</sup> and scanning electron microscopy (SEM),<sup>25</sup> have been used to study bitumen, asphaltenes, and/or oil sands tailings. However, these techniques have various shortcomings. SEM and TEM require extensive sample preparation and working under vacuum and a depressed temperature, which can alter the tailings' chemical structure.<sup>25</sup> Although AFM does not require much sample preparation, it reveals surface features only, without material specificity.<sup>16</sup> All of the above methods are not specific toward organic materials, and hence, the organic interaction with clay and their morphology is inferred but not known. However, fluorescence microscopy has shown excellent promise in imaging *in situ* bitumen/asphaltene structures at the micrometer scale without much sample preparation.<sup>26–29</sup>

In this article we report use of fluorescence microscopy to image bitumen in MFT. The fluorescence phenomena in MFT are depicted in Figure 1, where a bitumen–clay interface is illuminated with a laser to excite bitumen molecules to higher energy levels. The excited molecules then emit fluorescence while returning to the ground level. Because only bitumen shows natural fluorescence,<sup>30,19</sup> the exact bitumen location on clay can be imaged using fluorescence microscopy. Because bitumen is dispersed throughout the bulk of the sample, fluorescence from deeper planes creates significant background noise, resulting in the loss of information from the focused region of the sample. For that reason, to image bitumen distribution in MFT, we adapted a Total Internal Reflection Fluorescence (TIRF), which until now was used only in cell-biology research,<sup>31–33</sup> to image bitumen distribution in MFT. In TIRF, the sample is illuminated by an evanescent wave near the surface, in contrast to illumination by a propagating wave in a conventional confocal fluorescence microscope. The illumination depth in TIRF can be made as small as 100 nm to eliminate the background noise, enabling imaging of detailed features. TIRF can provide information on bitumen distribution and the bitumen–clay interaction in tailings in real time,

showing the effect of change in the temperature, pressure, flocculants, and pH.<sup>34,35</sup>

First, we present the fluorescence excitation and emission spectra and show that it is possible to observe the bitumen–clay and bitumen–water interfaces using confocal epifluorescence microscopy. Then, we show the distribution of bitumen in MFT using TIRF images. Finally, using high-resolution TIRF microscopy, we provide novel insights on the spatial location of residual bitumen on clay agglomerates in diluted MFT samples. Understanding bitumen distribution on clay and how it affects the clay–clay interaction in MFT is crucial for the development of more effective chemicals and processes to accelerate particle aggregation and sedimentation.

## 2. EXPERIMENTAL SECTION

Pure kaolin model clay, Athabasca bitumen, and MFT were provided by the Institute of Oil Sands Innovation (IOSI), University of Alberta.

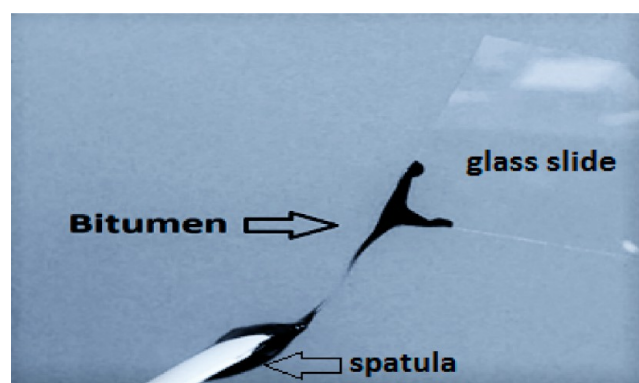


Figure 2. Athabasca bitumen that was observed using epifluorescence microscopy techniques.

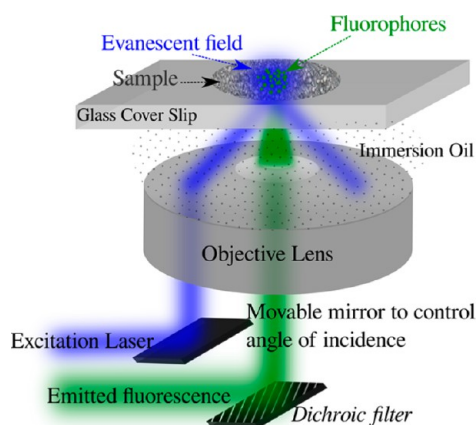


Figure 3. Kaolin (model clay) used to observe the fluorescence intensity difference between bitumen and clay.



Figure 4. MFT sample from Syncrude tailings pond.

Athabasca bitumen used in the spectrofluorometer and confocal epifluorescence microscopy experiments was obtained from Syncrude Canada, Ltd. It was produced by the hot-water extraction process and contained about 4–5 wt % asphaltenes.



**Figure 5.** TIRF microscope schematic. The sample is illuminated by evanescent fields near the surface of the coverslip.

The MFT samples used in the confocal epifluorescence microscopy and TIRF experiments were obtained in 2014 from Syncrude Canada, Ltd. tailings ponds. These MFT samples contain approximately 31 wt % solids, 4 wt % bitumen, and 65 wt % water.

Confocal epifluorescence microscopy and TIRF do not require an elaborate procedure for sample preparation. The sample preparations simply involved preparing the glass slides.

**2.1. Spectrofluorometer.** Laser source and excitation filters used to image bitumen, asphaltenes, and tailings are indicated in past literature. As a result of some discussions about the excitation wavelength of various bitumen components in these literature,<sup>26</sup> confirming the favorable laser source was deemed necessary for our TIRF experiments. A spectrofluorometer was chosen for this purpose.

A Varian Cary Eclipse spectrofluorometer was used to obtain the excitation and emission spectra with respect to fluorescence intensity for bitumen. These spectra aided to visualize the range of excitation and emission wavelengths over which bitumen can be easily detected using fluorescence techniques. Hence, narrowed down the favorable laser source and emission filter in TIRF for MFT imaging.

Dilute bitumen samples with concentrations of 0.1, 0.3, and 0.5 g/L bitumen in toluene were made to obtain these spectra. This was necessary because the spectrofluorometer is known to give better results for dilute samples. As a result of the inner filter effect,<sup>36</sup> at a high sample concentration there is high excitation light scattering and internal absorption of fluorescence, leading to the loss of fluorescence intensity in the resulting spectra. As a result, it is necessary to use dilute samples.<sup>37</sup>

A constant quantity (4 mL) of these samples was taken in a glass cuvette to ensure repeatability of results.

**2.2. Confocal Epifluorescence Microscope.** The fluorescence microscope is an optical microscope that uses a high-intensity light source to illuminate a sample, which then emits fluorescence. Fluorescence from the sample is always of higher wavelength than that of the excitation wavelength. A dichroic mirror and an emission

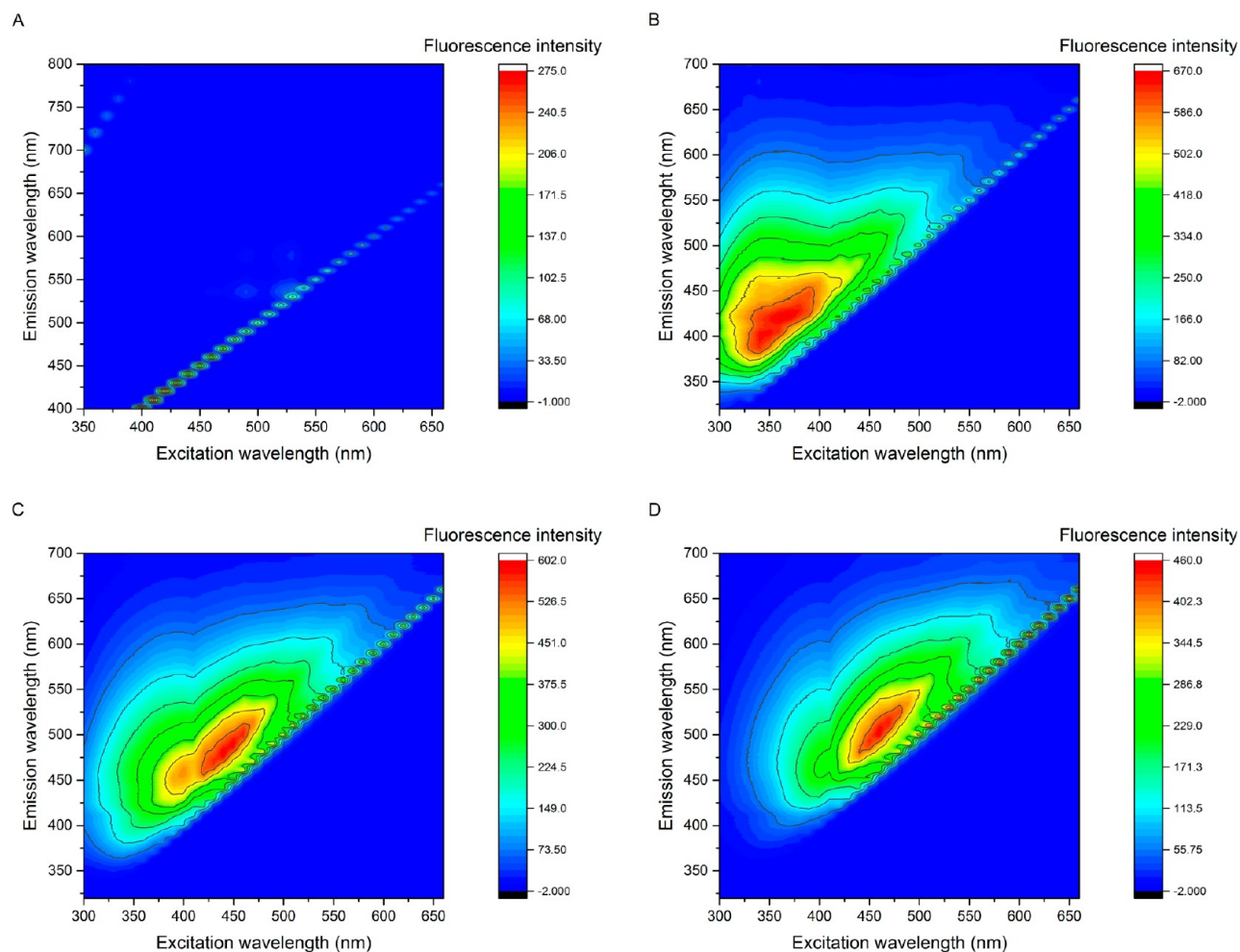


**Figure 6.** Image A shows a spectrofluorometer graph depicting the change in fluorescence intensity for a range of excitation and emission wavelengths for a 4 mL sample of toluene. Images B, C, and D show this graph for 0.1, 0.5, and 0.3 g/L bitumen in toluene, respectively.

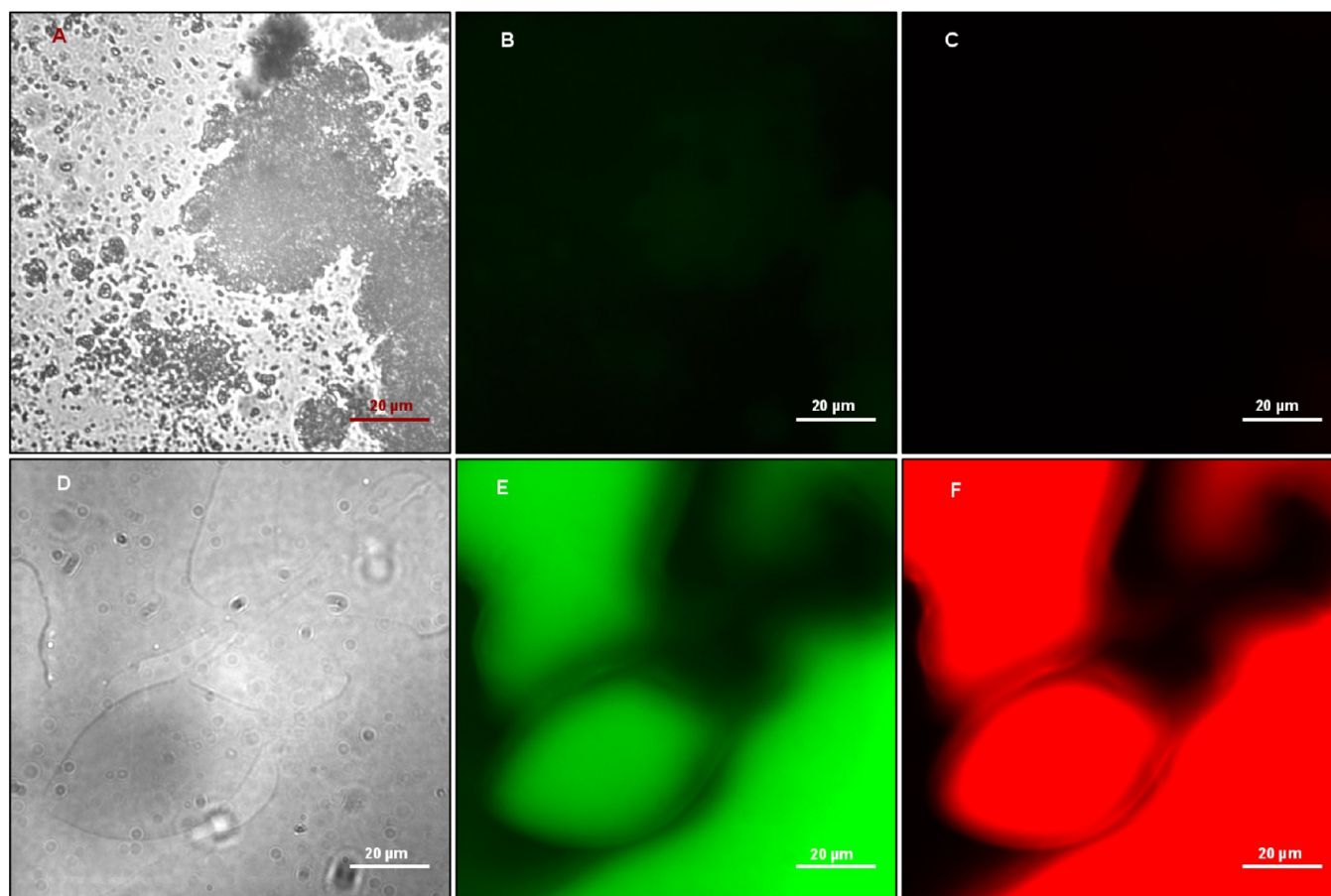


**Figure 7.** Images A and D represent the bright-field image of kaolin and Athabasca bitumen, respectively. Images B and E show the epifluorescence images of clay and Athabasca bitumen, respectively, for excitation with a xenon lamp and emission filter of 500–550 nm. Images C and F show the epifluorescence images of clay and Athabasca bitumen, respectively, for excitation with a xenon lamp and emission filter of 560–640 nm. Clay is not showing substantial fluorescence compared to the strong fluorescence of bitumen.

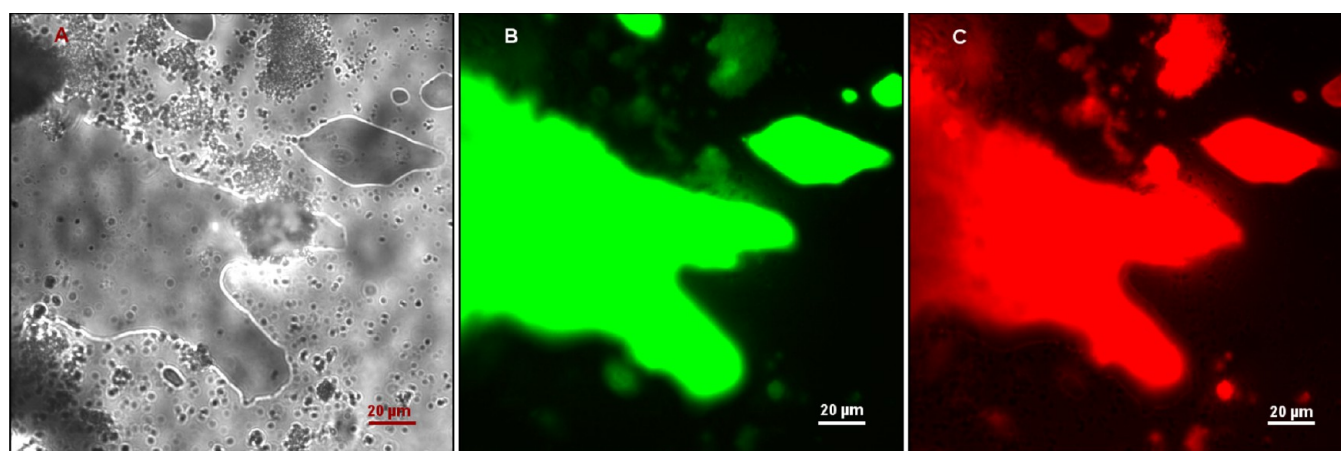


**Figure 8.** Image A shows a bright-field image of the clay and bitumen interface. Image B shows the fluorescence image of the clay and bitumen interface for excitation with a xenon lamp and emission filter of 500–550 nm. Image C shows the fluorescence image of the clay and bitumen interface for excitation with a xenon lamp and emission filter of 560–640 nm. A clear clay and bitumen interface is visible with epifluorescence.

filter can allow emitted wavelength to pass through. A condenser and an objective then collect the wavelength.

A more efficient form of the fluorescence microscope, the epifluorescent microscope enables illumination and detection to take place on the same side of the sample. This ensures that only reflected excitation light and emitted light are collected by the objective, which drastically increases the signal-to-noise ratio.<sup>38</sup>

The advantages of using any type of fluorescence microscopy for oil-sands-related research is that this technique is organic-specific, which is not the case with most other techniques being used currently. It is also a non-destructive method and can provide measurements with respect to time.<sup>38</sup>

Past studies have indicated that bitumen shows natural fluorescence.<sup>26,30</sup> Hence, using dyes to tag bitumen is not necessary. This is another advantage of the fluorescence microscopy technique.

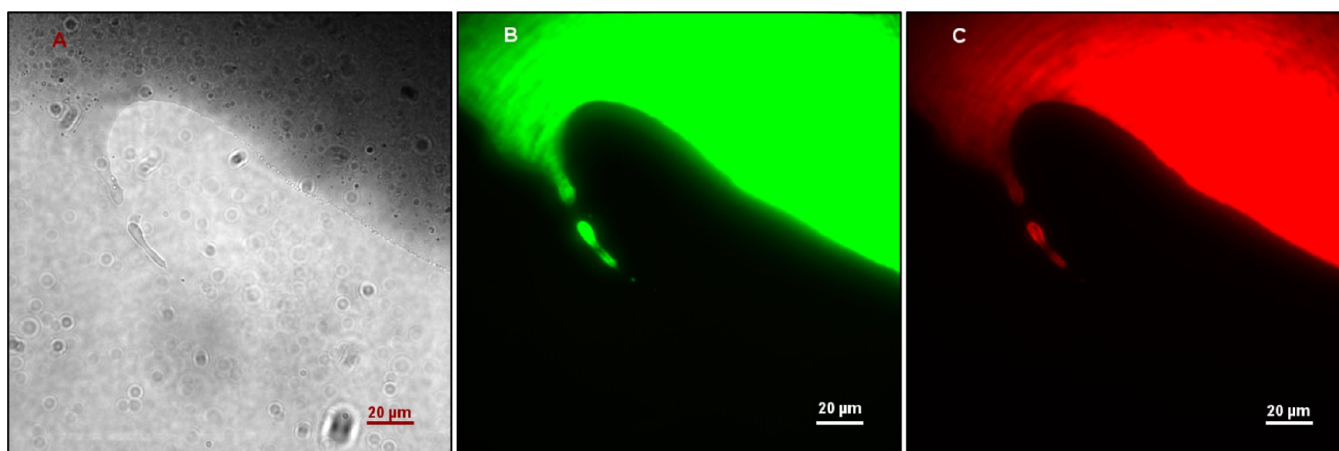


**Figure 9.** Image A shows a bright-field image of the water and bitumen interface. Image B shows the fluorescence image of the water and bitumen interface for excitation with a xenon lamp and emission filter of 500–550 nm. Image C shows the fluorescence image of the water and bitumen interface for excitation with a xenon lamp and emission filter of 560–640 nm. The water and bitumen interface is clearly seen with epifluorescence.

The epifluorescence microscope has the objective at the bottom of the sample holder. Consequently, the glass cover had to be placed on the bottom side. All slides were prepared by first placing the sample on the glass cover and then covering the sample with a glass to prevent any possible air gap between the glass cover and the sample. An air gap is not favorable because the refractive index of air ( $\sim 1$ ) is lower than the refractive index of the glass cover, objective lens, and immersion oil ( $\sim 1.52$  for all three), which leads to distortion of the images.

The model clay–bitumen interface sample, bitumen–water interface sample, individual bitumen (as shown in Figure 2), model clay samples (as shown in Figure 3), MFT (as shown in Figure 4), and dilute MFT sample slides were prepared and imaged using an epifluorescence microscope with a xenon lamp source and emission filters in the range of 500–550 nm (green) and 560–640 nm (red). The confocal feature of the epifluorescence microscope made it possible to capture the fluorescence image Z-stack for the MFT samples, which gave information about the shape of the fluorescing particles and also presented the possibility to perform quantitative analysis for changes in the bitumen distribution on clay with variations in temperature, pressure, and flocculants.

**2.3. TIRF Microscope.** In a conventional epifluorescence microscope, the entire sample is flooded with excitation light, resulting in fluorescence from all planes. This obscures details in the captured images. In TIRF, the excitation laser is made incident on the glass coverslip at an angle greater than its critical angle, as shown in Figure 5. As a result, the incident laser undergoes total internal reflection, and only an evanescent field develops adjacent to the glass–sample interface and decays exponentially away from it. The depth of the evanescent field can be controlled by controlling the incident angle. This depth can be made as small as 100 nm, eliminating any noise from deeper planes. The objective lens then collects the light emitted by the fluorophores and a digital camera is used to form the resulting image. This technique can generate a very high-contrast images.

Samples prepared for epifluorescence microscopy were also used for TIRF microscopy. The TIRF facility had 488, 543, and 633 nm laser sources. The emission filters used for the 488, 543, and 633 nm excitation lasers were in the ranges of 500–550 nm (green), 560–640 nm (red), and 650–730 nm (red), respectively. To obtain good TIRF images, the incidence angle was made slightly greater than the critical angle.

### 3. RESULTS AND DISCUSSION

**3.1. Spectrofluorometer.** The spectrofluorometer experiments helped to narrow down the laser source and filter cubes for the confocal epifluorescence microscope and TIRF microscope experiments. The results obtained from the

spectrofluorometer were plotted in the form of color contour maps to help visualize the results.

Because toluene was used to prepare the diluted bitumen samples, it was important to obtain excitation and emission spectra data for toluene to make sure that fluorescence from toluene would not interfere with fluorescence from the bitumen. It can be observed in Figure 6A that toluene did not show any substantial fluorescence in the excitation and emission wavelength ranges of interest.

The graphs for 0.1, 0.3, and 0.5 g/L concentrations of Athabasca bitumen containing about 4–5 wt % asphaltenes can be seen in the images B, C, and D of Figure 6, respectively. The spectrofluorometer results showed that the peak excitation wavelength was in the range of 350–500 nm and the peak emission wavelength was in the range of 400–550 nm for the 0.1, 0.3, and 0.5 g/L concentrations of bitumen. These data are in agreement with the literature.<sup>26–30</sup> As expected, an increased first-order scattering was observed with an increase in the sample concentration. Taking the spectrofluorometer results into consideration, a 488 nm laser source and 500–550 nm emission filter from the available resources were found to be the best choices for the confocal epifluorescence microscope and TIRF microscope imaging.

**3.2. Confocal TIRF and Epifluorescence Microscope.** Bitumen and clay sample images were taken using bright-field and epifluorescence microscopies. Samples of bitumen were prepared by smearing a thin film of bitumen on the glass cover. The thin film/strands of bitumen made it possible to image it with a bright-field microscope. Samples of kaolin (model clay) were prepared by sprinkling Kaolin powder on the glass cover. The bright-field images of clay and bitumen can be seen in images A and D of Figure 7, respectively. Figure 7D shows that the lack of contrast makes it difficult to observe bitumen. Bitumen can be clearly observed as a result of its strong fluorescence in images E and F of Figure 7. However, Figure 7B and C shows that clay cannot be clearly seen, because it lacks substantial fluorescence.

The fluorescence intensities of bitumen and kaolin samples (Figure 7) were compared at the same camera settings in an epifluorescence microscope. These settings were noted and used for MFT samples, ensuring that bitumen and clay could be distinguished in these samples.

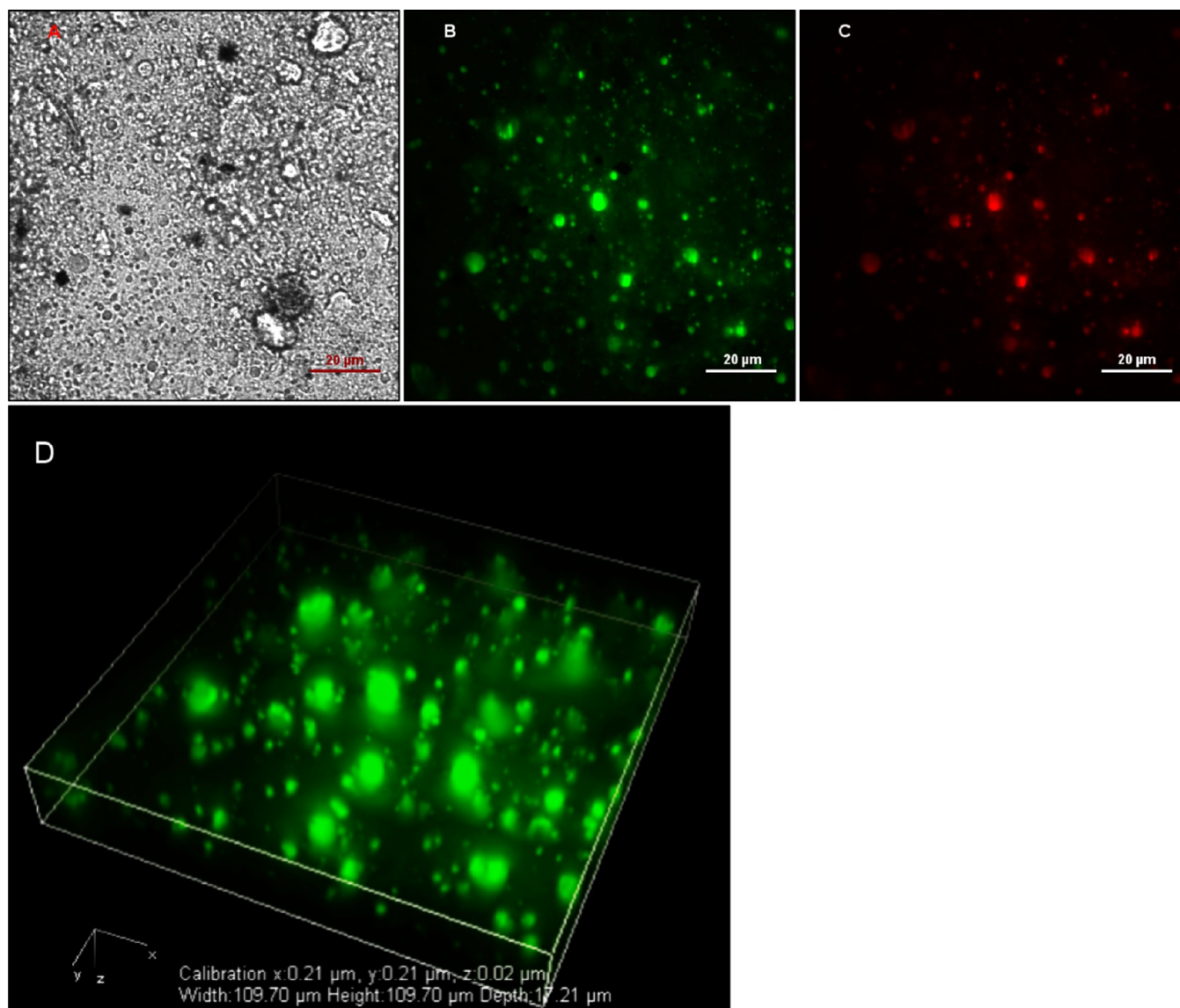


**Figure 10.** Image A shows a bright-field image of the MFT sample. Image B shows the TIRF images of the MFT sample for an excitation laser of 488 nm and emission filter of 500–550 nm, and image C shows the TIRF image of the MFT sample for an excitation laser of 543 nm and emission filter of 560–640 nm. MFT sample fluorescence images indicate that the fluorescing bitumen particles dispersed in non-fluorescing clay and water. Image D shows 3D reconstruction of the MFT sample at the same location and settings as image B.

Samples with the bitumen and clay interface were prepared by smearing the bitumen strands on the glass cover and sprinkling some kaolin around it. The clay and bitumen interface could be clearly observed using epifluorescence microscopy, as seen in Figure 8. These images confirm that bitumen and clay can be distinguished using fluorescence techniques.

The water and bitumen sample slides were prepared by smearing the bitumen strands on the glass cover and then adding some water. These sample images were observed using an epifluorescence microscope. Figure 9 shows that water did not show fluorescence and the bitumen/water interface could be clearly distinguished. The fluorescence images for bitumen/clay and bitumen/water confirmed that bitumen would be clearly seen in MFT sample fluorescence images.

In the case of the MFT sample, both fluorescence images and bright-field images were important. The bright-field image showed the location of clay particles in the sample, while the

fluorescence images showed the location of bitumen. The MFT sample was prepared by smearing a thin film onto the glass cover. The thin film enabled imaging with a bright-field microscope. Figure 10B and C show the fluorescence images of the MFT sample showed fluorescing particles in a pool of non-fluorescing media. The conclusion drawn from imaging the bitumen–clay and bitumen–water interfaces, it is understood that the fluorescing particles were bitumen and non-fluorescing media were water and clay combined. However, as a result of a high concentration of clay particles in these MFT samples, it was difficult to clearly observe clay particle boundaries in the bright-field images of MFT samples. Figure 10A did not clearly show whether the bitumen was attached to the clay, suspended in water, or both. To overcome this information deficit, the MFT sample was diluted.

The three-dimensional (3D) image seen in Figure 10D helped to clarify the shape of the fluorescing particles.

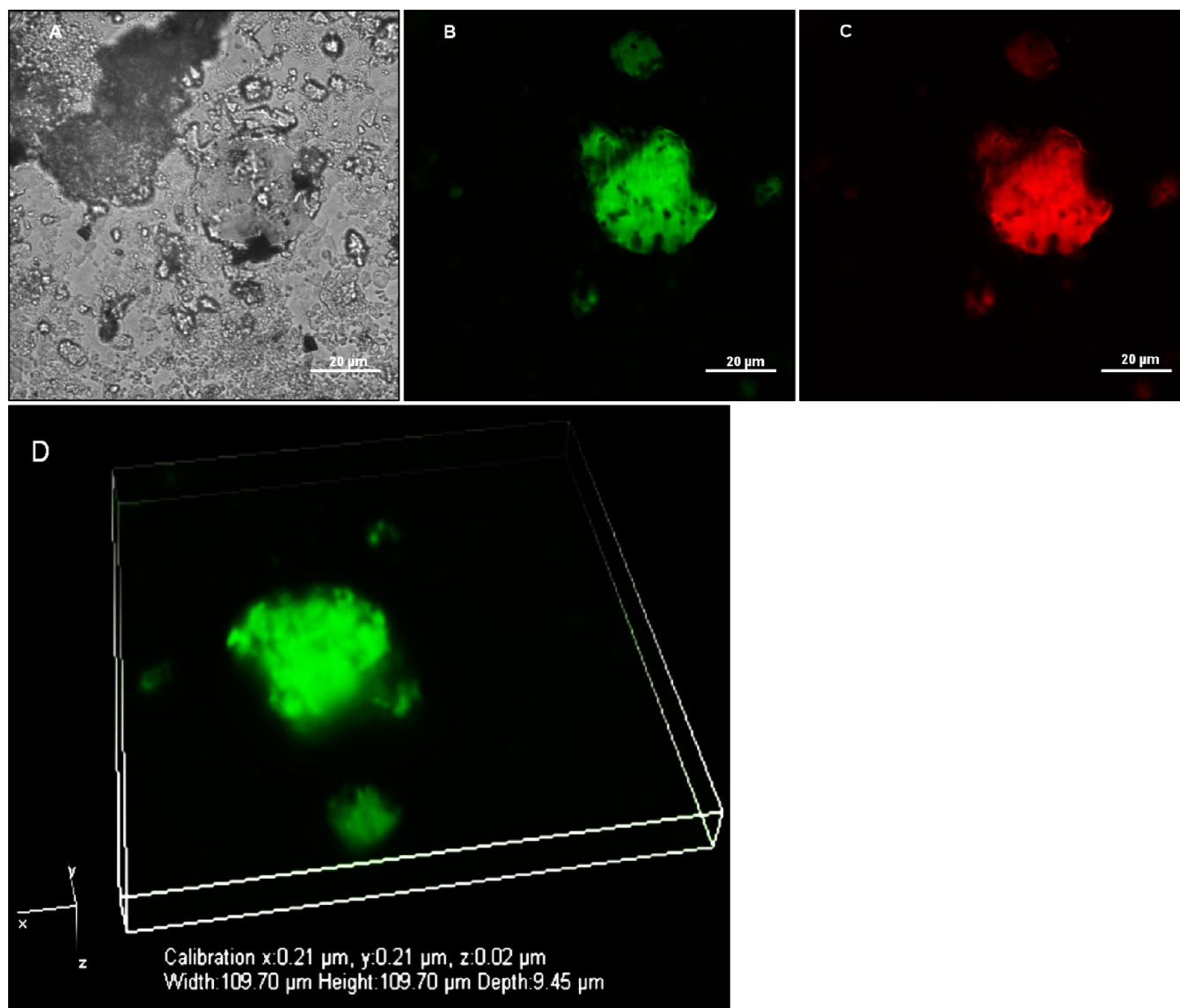


**Figure 11.** Image A shows a bright-field image of the diluted MFT sample. Image B shows the TIRF images of the diluted MFT sample for an excitation laser of 488 nm and emission filter of 500–550 nm, and image C shows the TIRF image of the diluted MFT sample for an excitation laser of 543 nm and emission filter of 560–640 nm. The diluted MFT sample fluorescence image shows fluorescing bitumen particles near the clay particle location in the bright-field image. Image D shows 3D reconstruction of the diluted MFT sample at the same location and settings as image B.

Diluted MFT samples were prepared by first diluting 1 g of MFT with about 100 mL of deionized water at 60 °C. A drop of this diluted MFT was added to the glass cover, allowed to dry, and covered with a glass slide. As seen in Figure 11A, the bright-field image of diluted MFT samples helped to observe that a single layer of clay aggregated and reduced the density of clay particles, which previously obscured details. It showed the two-dimensional (2D) shape of clay aggregates and also helped to better understand the bitumen coverage on clay. These samples were easier to observe under a bright field, and noise was greatly reduced in these images as a result of a lower concentration of clay particles. The fluorescence images B and C of Figure 11 show the bitumen near the clay particles in the bright-field image. Figure 11D shows a 3D reconstruction of the diluted MFT sample at the same location as the 2D images. This image gives an idea of the shape of the bitumen-coated clay aggregates. The 3D images can be used for future image

analysis to find the surface coverage of bitumen on clay aggregates.

All of the fluorescence images in this paper were taken at the same camera settings, with exposure time set at 200 ms and exposure multiplier set at 100, to help maintain consistency in the results.

Figure 12 shows various bright-field images and fluorescence images of diluted MFT samples, which were superimposed using ImageJ software to observe the bitumen surface coverage on the clay particles. In Figure 12, the dark gray particles are clay<sup>39</sup> and green dots are bitumen. In this sample of MFT, bitumen is not suspended freely in water. Residual bitumen is bridging and coating the clay agglomerates. It can also be seen that only some percentage of clay aggregates is associated with bitumen, confirming the presence of water-wet and bitumen-wet clays in MFT.

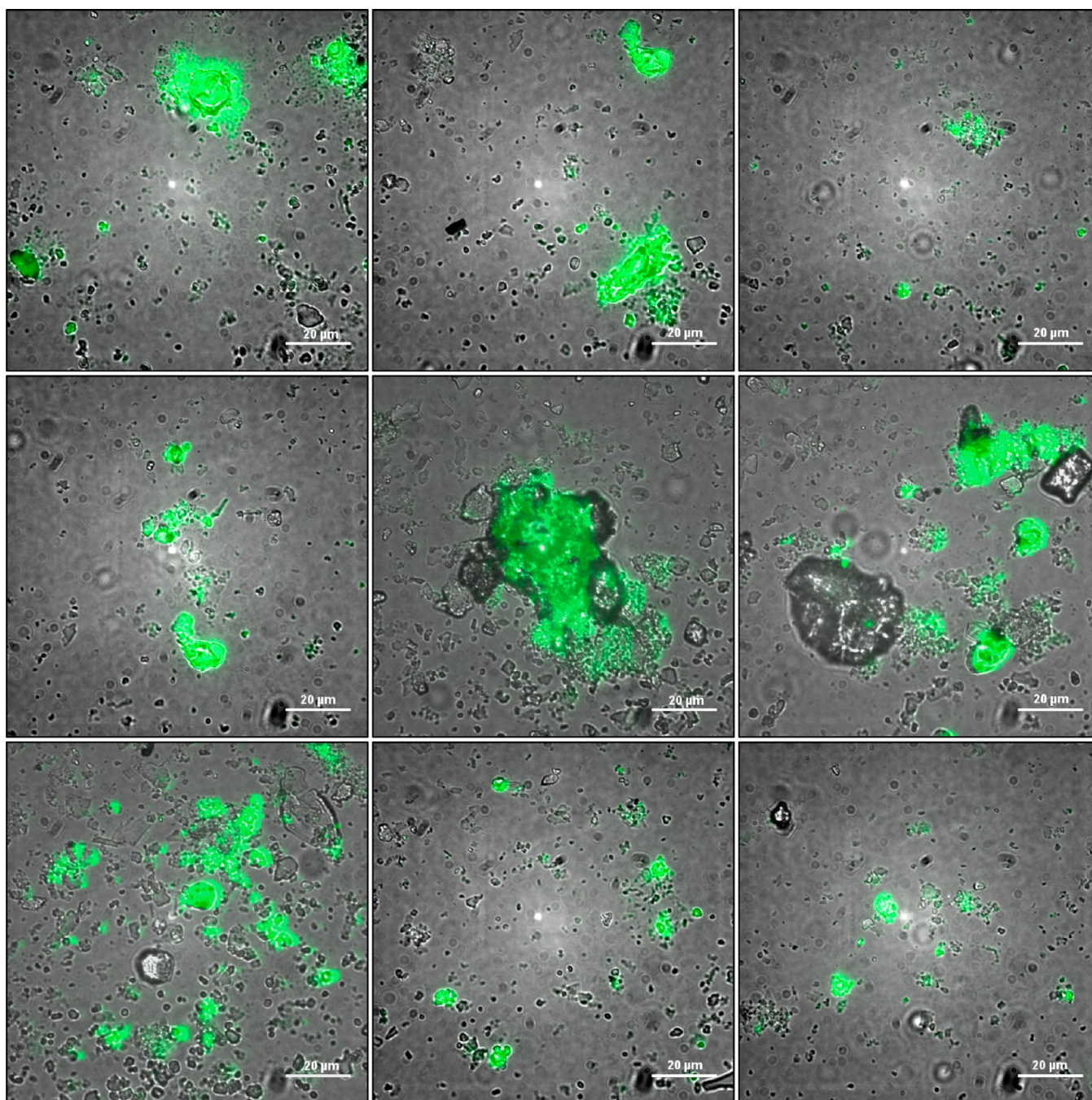


**Figure 12.** Superimposed bright-field and 488 nm excitation laser TIRF images of the diluted MFT sample. The dark gray particles in these images are clay particles, while the green dots are bitumen.

#### 4. CONCLUSION

Most previous methods have been able to map MFT samples with only predictions about the bitumen location. This was mainly due to the use of inorganic-specific techniques.<sup>1</sup> The high-resolution and organic-specific TIRF microscope images discussed in this paper help to map the exact location and surface coverage of bitumen on fine clay in MFT. These images also make it possible to observe the presence of water-wet clay particles, along with the bitumen-wet clay particles. They also shed light on the bitumen–clay particle boundaries and surfaces, which can be even more clearly visualized with the aid of edge detection techniques in image analysis. At 0.3  $\mu\text{m}$  resolution, the images also show that bitumen coats some clay

and bridges some clay aggregates together, as conceptually visualized in previous literature.<sup>2</sup> There was no free bitumen observed in the bulk of the MFT sample at the current resolution.

The resolution of images can be further improved using metamaterial substrate instead of a glass coverslip.<sup>40</sup> Imaging the bitumen coverage on clay and observing its effect on the clay–clay interaction will aid in the development of techniques to accelerate clay agglomeration/sedimentation and enhance bitumen recovery in the future.

## AUTHOR INFORMATION

### Corresponding Author

\*E-mail: [nn1@ualberta.ca](mailto:nn1@ualberta.ca).

### Notes

The authors declare no competing financial interest.

## ACKNOWLEDGMENTS

The authors are grateful for the financial support of the IOSI. The authors are also thankful to Dr. Xiaoli Tan for his help with obtaining samples and some great technical discussions. The authors also acknowledge the use of facilities at the Oil Sands and Coal Interfacial Engineering Facility (OSCIEF), equipment at the National Institute for Nanotechnology (NINT), University of Alberta, and biological services equipment at the Department of Chemistry, University of Alberta.

## NOMENCLATURE

MFT = mature fine tailings  
 TIRF = total internal reflection fluorescence  
 SEM = scanning electron microscopy  
 TEM = transmission electron microscopy  
 AFM = atomic force microscopy  
 PMT = photomultiplier tube

## REFERENCES

- Masliyah, J. H.; Xu, Z.; Czarnecki, J. A.; Dabros, M. *Handbook on Theory and Practice of Bitumen Recovery from Athabasca Oil Sands*; Kingsley Knowledge Publishing: Edmonton, Alberta, Canada, 2011; Vol. 1.
- Sparks, B. D.; Kotlyar, L. S.; O'Carroll, J. B.; Chung, K. H. Athabasca oil sands: Effect of organic coated solids on bitumen recovery and quality. *J. Pet. Sci. Eng.* **2003**, *39* (3–4), 417–430.
- Scott, A. C.; MacKinnon, M. D.; Fedorak, P. M. Naphthenic acids in athabasca oil sands tailings waters are less biodegradable than commercial naphthenic acids. *Environ. Sci. Technol.* **2005**, *39* (21), 8388–8394.
- Folwell, B. D.; McGenity, T. J.; Price, A.; Johnson, R. J.; Whitby, C. Exploring the capacity for anaerobic biodegradation of polycyclic aromatic hydrocarbons and naphthenic acids by microbes from oil-sands-process-affected waters. *Int. Biodeterior. Biodegrad.* **2016**, *108*, 214–221.
- Holden, A. A.; Haque, S. E.; Mayer, K. U.; Ulrich, A. C. Biogeochemical processes controlling the mobility of major ions and trace metals in aquitard sediments beneath an oil sand tailing pond: Laboratory studies and reactive transport modeling. *J. Contam. Hydrol.* **2013**, *151*, 55–67.
- Wang, X. W.; Feng, X.; Xu, Z.; Masliyah, J. H. Polymer aids for settling and filtration of oil sands tailings. *Can. J. Chem. Eng.* **2010**, *88* (3), 403–410.
- Yang, W. Y.; Qian, J. W.; Shen, Z. Q. A novel flocculant of Al(OH)<sub>3</sub>-polyacrylamide ionic hybrid. *J. Colloid Interface Sci.* **2004**, *273* (2), 400–405.
- Mpofu, P.; Addai-Mensah, J.; Ralston, J. Investigation of the effect of polymer structure type on flocculation, rheology and dewatering behaviour of kaolinite dispersions. *Int. J. Miner. Process.* **2003**, *71* (1–4), 247–268.
- Li, H.; Long, J.; Xu, Z.; Masliyah, J. H. Novel polymer aids for low-grade oil sand ore processing. *Can. J. Chem. Eng.* **2008**, *86* (2), 168–176.
- Masliyah, J.; Zhou, Z. J.; Xu, Z.; Czarnecki, J.; Hamza, H. Understanding Water-Based Bitumen Extraction from Athabasca Oil Sands. *Can. J. Chem. Eng.* **2004**, *82* (4), 628–654.
- Boxill, L. Potential for use of methylene blue index testing to enhance geotechnical characterization of oil sands ores and tailings. *Proceedings of the Tailings and Mine Waste*; Vancouver, British Columbia, Canada, Nov 6–9, 2011.
- Tamiz Bakhtiari, M.; Harbottle, D.; Curran, M.; et al. Role of Caustic Addition in Bitumen–Clay Interactions. *Energy Fuels* **2015**, *29* (1), 58–69.
- Mercier, P. H. J.; Ng, S.; Moran, K.; et al. Colloidal Clay Gelation: Relevance to Current Oil Sands Operations. *Pet. Sci. Technol.* **2012**, *30* (9), 915–923.
- Yin, X.; Miller, J. D. Wettability of kaolinite basal planes based on surface force measurements using atomic force microscopy. *Miner. Metall. Process.* **2012**, *29* (1), 8.
- Kaminsky, H. A. W.; Etsell, T. H.; Ivey, D. G.; Omotoso, O. Distribution of clay minerals in the process streams produced by the extraction of bitumen from Athabasca oil sands. *Can. J. Chem. Eng.* **2009**, *87* (1), 85–93.
- Liu, J.; Xu, Z.; Masliyah, J. Role of fine clays in bitumen extraction from oil sands. *AIChE J.* **2004**, *50* (8), 1917–1927.
- Klein, C. Effect of Residual Bitumen on Polymer-Assisted Flocculation of Fluid Fine Tailings. M.S. Dissertation, University of Alberta, Edmonton, Alberta, Canada, 2014.
- Dang-Vu, T.; Jha, R.; Wu, S.-Y.; Tannant, D. D.; Masliyah, J.; Xu, Z. Effect of solid wettability on processability of oil sands ores. *Energy Fuels* **2009**, *23* (5), 2628–2636.
- Muñoz, V. a.; Kasperski, K. L.; Omotoso, O. E.; Mikula, R. J. The Use of Microscopic Bitumen Froth Morphology for the Identification of Problem Oil Sand Ores. *Pet. Sci. Technol.* **2003**, *21* (9–10), 1509–1529.
- Hooshari, A.; Uhlík, P.; Kaminsky, H. W.; et al. High resolution transmission electron microscopy study of clay mineral particles from streams of simulated water based bitumen extraction of Athabasca oil sands. *Appl. Clay Sci.* **2010**, *48* (3), 466–474.
- Osacky, M.; Geramian, M.; Ivey, D. G.; Liu, Q.; Etsell, T. H. Influence of Nonswelling Clay Minerals (Illite, Kaolinite, and Chlorite) on Nonaqueous Solvent Extraction of Bitumen. *Energy Fuels* **2015**, *29* (7), 4150–4159.
- Johnston, C. T. Probing the nanoscale architecture of clay minerals. *Clay Miner.* **2010**, *45* (3), 245–279.
- Marshall, G. M.; Kingston, D. M.; Moran, K.; Mercier, P. H. J. Multivariate factor analysis of heavy minerals concentrate from Athabasca oil sands tailings by X-ray photoelectron spectroscopy. *Surf. Interface Anal.* **2014**, *46*, 197.
- Osacky, M.; Geramian, M.; Dyar, M. D.; Sklute, E. C.; Valter, M.; Ivey, D. G.; Liu, Q.; Etsell, T. H.; et al. Characterisation of petrologic end members of oil sands from the Athabasca region, Alberta, Canada. *Can. J. Chem. Eng.* **2013**, *91* (8), 1402.
- Hooshari, A.; Uhlík, P.; Ivey, D. G.; Liu, Q.; Etsell, T. H. Clay minerals in nonaqueous extraction of bitumen from Alberta oil sands: Part 2. Characterization of clay minerals. *Fuel Process. Technol.* **2012**, *96*, 183–194.
- Bearsley, S.; Forbes, A.; Haverkamp, R. G. Direct observation of the asphaltene structure in paving-grade bitumen using confocal laser-scanning microscopy. *J. Microsc.* **2004**, *215* (2), 149–155.
- Hung, J.; Castillo, J. A.; Reyes, A. Colloidal structural evolution of asphaltene studied by confocal microscopy. *Proc. SPIE* **2004**, *5622*, 154–159.
- Franco, J. C.; Gonçalves, G.; Souza, M. S.; et al. Towards in situ fluorescence spectroscopy and microscopy investigations of asphaltene precipitation kinetics. *Opt. Express* **2013**, *21* (25), 30874.
- Stasiuk, L. D.; Gentzis, T.; Rahimi, P. Application of spectral fluorescence microscopy for the characterization of Athabasca bitumen vacuum bottoms. *Fuel* **2000**, *79* (7), 769–775.
- Mikula, R. J.; Munoz, V. a. Characterization of emulsions and suspensions in the petroleum industry using cryo-SEM and CLSM. *Colloids Surf., A* **2000**, *174*, 23–36.
- Boulanger, J.; Gueudry, C.; Münch, D.; et al. Fast high-resolution 3D total internal reflection fluorescence microscopy by incidence angle scanning and azimuthal averaging. *Proc. Natl. Acad. Sci. U. S. A.* **2014**, *111* (48), 17164–17169.
- Knight, A. E. Single-molecule fluorescence imaging by total internal reflection fluorescence microscopy (IUPAC Technical Report). *Pure Appl. Chem.* **2014**, *86* (8), 1303–1320.

- (33) Shen, H.; Huang, E.; Das, T.; Xu, H.; Ellisman, M.; Liu, Z. TIRF microscopy with ultra-short penetration depth. *Opt. Express* **2014**, *22* (9), 10728–10734.
- (34) Amann, K. J.; Pollard, T. D. Direct real-time observation of actin filament branching mediated by Arp23 complex using total internal reflection fluorescence microscopy. *Proc. Natl. Acad. Sci. U. S. A.* **2001**, *98* (26), 15009–15013.
- (35) Nazemifard, N.; Bhattacharjee, S.; Masliyah, J. H.; Harrison, D. J. Nonmonotonous variation of DNA angular separation during asymmetric pulsed field electrophoresis. *Electrophoresis* **2013**, *34* (17), 2453–2463.
- (36) Yappert, M. C.; Ingle, J. D. Correction of Polychromatic Luminescence Signals for Inner-Filter Effects. *Appl. Spectrosc.* **1989**, *43* (5), 759–767.
- (37) Brandt, M. *Spectrofluorometers and Fluorescence Phenomena*, 2010; [http://loci.wisc.edu/files/loci/Introduction\\_to\\_Spectrofluorometry.pdf](http://loci.wisc.edu/files/loci/Introduction_to_Spectrofluorometry.pdf) (accessed Jan 1, 2015).
- (38) Ishikawa-Ankerhold, H. C.; Ankerhold, R.; Drummen, G. P. C. Advanced Fluorescence Microscopy Techniques—FRAP, FLIP, FLAP, FRET and FLIM. *Molecules* **2012**, *17* (12), 4047–4132.
- (39) Hande, A. B. Accelerated Dewatering and Drying Treatment of Oil Sands Tailings by Electrical Resonant Auto-Transformer. M.S. Dissertation, University of Alberta, Edmonton, Alberta, Canada, 2014.
- (40) Starko-Bowes, R.; Atkinson, J.; Newman, W.; et al. Optical Characterization of Epsilon-Near-Zero, Epsilon-Near-Pole, and Hyperbolic Response in Nanowire Metamaterials. *J. Opt. Soc. Am. B* **2015**, *32* (10), 2074–2080.